EFFECT OF PROTRUSION SHAPE ON FILM COOLING PERFORMANCE FOR THE CYLINDRICAL HOLE EMBEDDED IN A CONTOURED CRATER

Wenzhuang WANG[1,2], Chao ZHANG[1, 2,*], Zhiting TONG[1,2]

[1] Tianjin Key Laboratory for Advanced Mechatronic System Design and Intelligent Control, School of Mechanical Engineering, Tianjin University of Technology, Tianjin 300384, P.R. China

[2] National Demonstration Center for Experimental Mechanical and Electrical Engineering Education (Tianjin University of Technology), Tianjin 300384, P.R. China

[*] Corresponding author; E-mail: czhangxj@163.com

The cratered film-cooling hole is regarded as one of the potential applications with high cooling performance and low cost. This study focuses on the influence of the protrusion shape for the contoured crater embedded in the cylindrical hole. Four protrusion shapes, i.e., arc, rectangle, trapezoid, and triangle, are considered. The cooling effectiveness, flow structure, and aerodynamic loss for the cratered holes at blowing ratios of 0.5-2.5 are obtained using the numerical method with the Shear Stress turbulence model. The numerical results indicate that the arc and triangle protrusion models provide better lateral coolant coverage and higher area-averaged cooling effectiveness at higher blowing ratios, attributed to the ascendant anti-kidney-shaped vortex pair. The rectangle protrusion model provides the lowest area-averaged cooling effectiveness because the kidney-shaped vortex pair dominates the downstream flow field. For the aerodynamic loss, the largest total pressure loss coefficient occurs for the rectangle protrusion model and nearly equivalent values for the other three protrusion models. The contoured cratered holes with arc and triangle protrusions are generally recommended.

Key words*: Film cooling; Cratered hole; Protrusion shape; Cooling effectiveness; Aerodynamic loss; Numerical simulation*

1. Introduction

The film cooling technique plays a key role in modern gas turbine blade cooling. Ever since the concept of film cooling was proposed by Goldstein [1] in the 1970s, many research activities have been carried out to enhance the cooling effectiveness, which aims to reduce coolant consumption. The discrete hole with a cylindrical shape was suggested as the appropriate one and then commonly applied in practice due to its simplicity and lower manufacturing cost. The early studies [2-5] revealed that the blowing ratio significantly influences the cylindrical hole's cooling performance. They concluded that the effectiveness tends to increase with the increase of blowing ratio when the blowing ratio is lower than 0.5 but deteriorates sharply when the blowing ratio exceeds 0.5. Impurities in the air can be blocked in some of the film holes, and it has been found that the lateral cooling effectiveness decreases as the blockage rate increases. Mist injection can lead to improved cooling performance [6].

The optimization of the inclination angle of the multiple rows of cooling holes has also been considered [7].

The fan-shaped hole is considered the most important achievement among many improved designs and is applied in the design of blade cooling configuration nowadays. Compared with the cylindrical hole, the difference of the fan-shaped hole is the lateral or/and streamwise expansions after the metering section [8]. Therefore, the hole exit area is significantly increased, and the decreased coolant jetting momentum induces the kidney-shaped vortex pair to decrease correspondingly. The variants of the fan-shaped holes were summarized in [9]. Although the fan-shaped holes could significantly improve the cooling effectiveness, the complicated geometry and costly manufacturing increased the application difficulty. In addition to the fan-shaped holes, some novel-shaped holes, for example, crescent hole [10], clover-shaped hole [11], Nekomimi hole [12], and combined hole [13] have been proposed successively. However, the practical applications of these novel cooling holes are still limited, considering their intricate geometry and high manufacturing cost.

To overcome the problem of high manufacturing cost, the modification based on the cylindrical hole assisted by the thermal barrier coating (TBC) technology may be a potential alternative [14]. Two pioneering concepts were proposed for the trenched hole by Bunker [15] and the cratered hole by Firc and Campbell [16]. When the TBCs are spraying on the blade surface, a consecutive trench or discrete crater can be formed using a different mask. Tran et al. [17] feared that the trenched hole might weaken the structural integrity, despite its higher cooling performance. Hence, efforts have been made further to improve the cooling performance for the cratered hole.

Lu et al. [18] performed an experimental comparison work among three variants of cratered holes, i.e., an acentric elliptic one, a concentric elliptic one, and a concentric circular one. They found that the cratered hole with an acentric elliptic shape gives the best cooling performance among the cratered holes studied. The cooling effectiveness improvement depends on the crater shape compared to the cylindrical hole. Khalatov et al. [19] numerically compared the cooling performance among the circular, hemispherical, and triangular cratered holes and found that the triangular cratered hole shows the highest cooling effectiveness. Khalatov et al. [20] further performed a comparison study for the triangular cratered hole, emphasizing the effect of the leading-edge shape. Their numerical results showed that the hole with a concavely curved leading edge improves the cooling effectiveness slightly compared to a straight leading edge. Kalghatgi and Acharya [21] proposed the contoured cratered hole design featured with a "V"-shaped protrusion for the leading edge and numerically validated its superiority to the cylindrical hole. They believed that the additional anti-kidney-shaped vortex pair, induced by the "V"-shaped protrusion, is the main reason for the wider lateral coolant spreading and the improved cooling effectiveness. The flow dynamics of the cylindrical hole embedded in the contoured crater were further analyzed using the large eddy simulation [22]. Note that all the cratered holes [18-21] were studied under the condition of a small lateral distance of 3D between two adjacent rows (D is the cylindrical hole diameter). An et al. [23] proposed a novel contoured cratered hole design with a concavely curved protrusion and a larger streamwise diffusion. The cooling effectiveness was measured using the pressure-sensitive paint technology for the cratered hole with a lateral distance of 5D. Their experimental data revealed that the cooling effectiveness of the contoured cratered hole studied greatly improves compared with the cylindrical hole but still falls behind the fan-shaped hole slightly. Bai and Zhang [24] explained the flow mechanism for the improved cooling performance of the cratered hole proposed in [23] and hold that the curved protrusions play a crucial

role in generating anti-kidney-shaped vortex pair. Fu et al. [25] emphasized the influence of the crater depth on the flow field and cooling effectiveness for the contoured cratered hole. Bai et al. [26] further performed the optimization shape design of the contoured cratered design at two blowing ratios of 0.5 and 1.5. It was shown that an appropriate combination of the geometrical parameters could improve 17.21% at a blowing ratio of 0.5 and 101.96% at a blowing ratio of 1.5, compared with the reference model. The aerodynamic losses were studied under various coolant feeding channels for the same contoured cratered hole [27].

The review of the previous studies indicates that the cratered hole with a concavely curved leading edge provides high cooling effectiveness. Besides, as Khalatov et al. [20] suggested, the proper design of the concavely curved leading edge can improve cooling effectiveness. Hence, the current paper focuses on the influence of the protrusion shape of the contoured crater. Four concave protrusion shapes are considered: arc, rectangle, trapezoid, and triangle. The flow structure, cooling effectiveness, and total aerodynamic loss are analyzed based on the numerical results.

2. Physical model and numerical setup

2.1. Physical model

The contoured cratered holes studied in the current study are shown in Fig. 1. A cylindrical hole with an inclination angle relative to the streamwise direction (X coordinate) is embedded in the contoured crater. The diameter of the cylindrical hole is denoted as D with a value of 4 mm. The crater has an invariable profile along the normal wall direction (Z coordinate). The depth of the crater is $0.6D$. The crater is expanded with a distance of $1.6D$ in the streamwise direction and a total width of $3.6D$ in the lateral direction (Y coordinate). The leading edge of the crater is composed of a concave protrusion edge in the middle and two straight lines alongside. The streamwise length and lateral width of the protrusion are $1.25D$ and $1.4D$, respectively. For the contoured cratered hole type in this study, Bai and Zhang [24] have pointed out that the arc protrusion at the trailing edge of the crater has a key role in the generation of a new anti-kidney-shaped vortex pair. And this anti-kidney-shaped vortex pair can promote the lateral coverage effect of coolant, which is very significant for the cooling effectiveness. Therefore, the paper proposes four variants of protrusion shapes for study, including arc, rectangle, trapezoid, and triangle. The effects of different protrusion shapes on the cooling performance of the film cooling are further analyzed. These four protrusions have the same streamwise length and lateral width. The length of the top side for the trapezoid protrusion is $0.7D$. Note that the geometrical parameters of the crated hole with an arc protrusion are similar to those for the model Case 6 in [23], omitting the inclined leading edge.

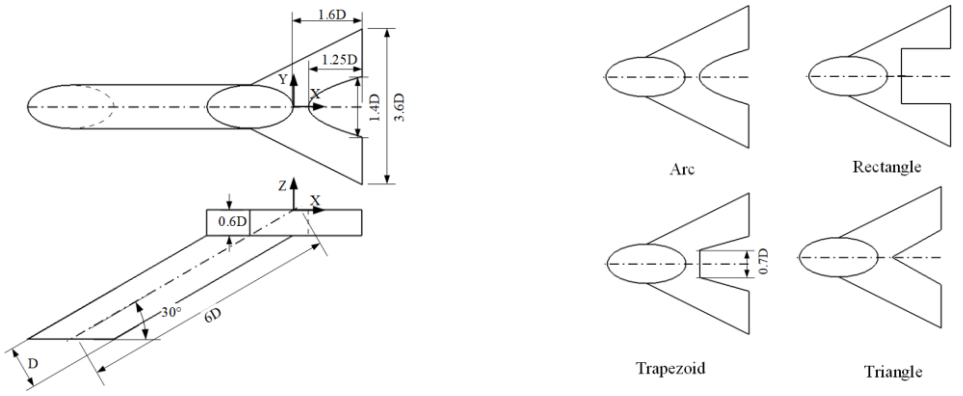

(a) Top view and cross-section view **(b) Four variants of protrusion shape**

Fig. 1 Contoured cratered cooling holes with various protrusion shapes

The computational domain is represented in Fig. 2, including the mainstream channel, the coolant plenum, and the cratered cooling hole. The mainstream channel has a total length of 80*D*, a width of 6*D*, and a height of 10*D*. The dimensions of the coolant plenum are 40*D*, 6*D*, and 10*D* in the streamwise, lateral normal-wall directions. The distance between the mainstream channel and the coolant plenum is 3*D* in the normal-wall direction. The hot air and coolant flow into the mainstream channel and coolant plenum along the coordinate *X*. The distance between the cylindrical hole exit and the mainstream channel inlet is 31*D*. The original point is located at the bottom wall surface of the mainstream channel. In the present study, only one row of the cratered hole is selected to mimic the finite rows of film-cooling holes with periodic boundaries. The downstream area ($0 \le X \le 30D$, $-3D \le Y \le 3D$) is the interesting region for evaluating the cooling effectiveness.

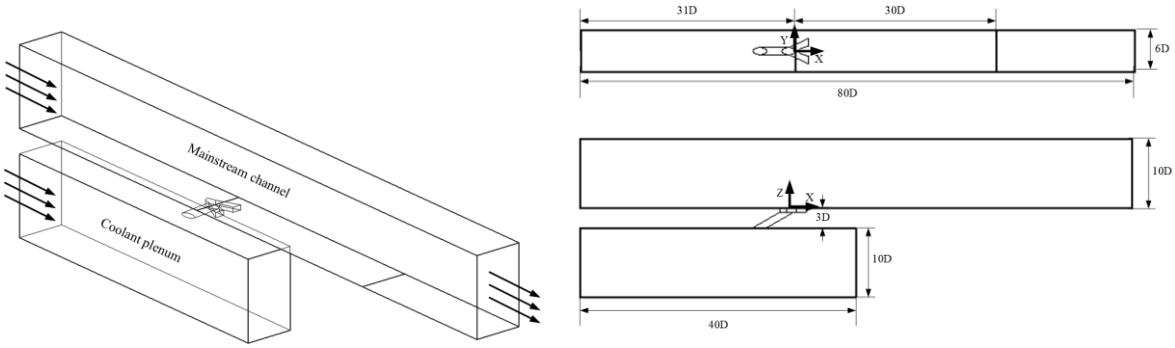

(a) Isometric view with boundary conditions **(b) Top view and cross-section view**

Fig. 2 Computational domain

The boundary conditions in the following simulations are almost identical to those in the experiment test [23]. The hot air flows into the mainstream channel with a uniform velocity of U_m=25 m/s, a temperature of T_m=414 K, and a turbulence intensity of 0.035. The static pressure condition of 1.0 bar is set at the mainstream channel outlet. The coolant enters the coolant plenum with a temperature T_c=300 K to keep the density ratio *DR*=1.38. The uniform velocity condition is also

imposed on the coolant plenum inlet, adjusted based on the given blowing ratios M=0.5-2.5. The definition formula of blowing ratio is given by:

$$M = DR \cdot \frac{U_c}{U_m} \tag{1}$$

where U_c is the mean velocity at the cross-section of the cylindrical hole part.

All the wall surfaces are set as smooth, adiabatic, and non-slip boundary conditions. The sidewalls (Y/D=-3 and 3) of the mainstream channel are set as transitional periodic boundary conditions.

2.2. Data reduction

In general, the dimensional form of the adiabatic wall temperature T_{aw} for the film-cooling, i.e., the cooling effectiveness η, is defined as:

$$\eta = \frac{T_m - T_{aw}}{T_m - T_c} \tag{2}$$

The area-averaged cooling effectiveness η_{av} in the interested region downstream the hole ($0 \le X/D \le 30$, $-3 \le Y/D \le 3$) is calculated as follows:

$$\eta_{av} = \frac{1}{6D \times 30D} \int_0^{30D} \int_{-3D}^{3D} \eta dY dX \tag{3}$$

The streamwise vortex intensity ω_X is calculated to represent the strength of the kidney-shaped or anti-kidney-shaped vortex pair, which is expressed as:

$$\omega_X = \frac{\partial U_Z}{\partial Y} - \frac{\partial U_Y}{\partial Z} \tag{4}$$

where U_Y, U_Z are the velocity components in the Y and Z directions, respectively.

The aerodynamic loss occurs inevitably in the mixing process between the coolant and the mainstream hot air. As suggested by Aga et al. [30], the total pressure loss coefficient is used as the evaluation criterion of the aerodynamic loss. The calculation expression is given by:

$$\xi = \frac{1}{\rho_m U_m{}^2 / 2} \left(\frac{m_c}{m_c + m_m} P_{t,cin} + \frac{m_m}{m_c + m_m} P_{t,m} - P_{t,f} \right) \tag{5}$$

where ρ_m, m_m, $P_{t,m}$ are the density, mass flow rate, and total pressure at the mainstream channel inlet, m_c is the mass flow rate of coolant, $P_{t,cin}$, $P_{t,f}$ are the mean total pressures at the cooling hole entrance and the mainstream channel outlet.

2.3. Grid independence test

The computational grids are generated using the software package ICEM CFD. As shown in Fig. 3, the grid points are clustered near the wall surfaces and around the hole to represent the boundary layer sufficiently. The height of the first grid away from the wall surfaces is nearby 0.005D, assuring that the value of Yplus is around 1. The stretching factor of the grid clustering is 1.3.

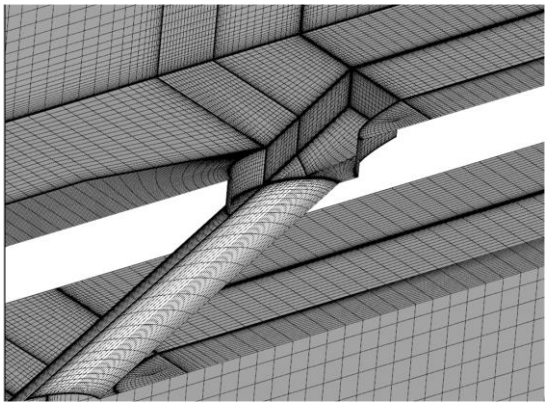

Fig. 3 Computational grid for the cratered hole with arc protrusion

Grid independence tests are performed to obtain the optimal grid level to trade-off the computational cost and result independence. Fig. 4 represents the grid independence test result, taking the cratered hole with arc protrusion at M=0.5 as an example. The dimensionless velocity profiles U/U_m along the line (X/D=5, Y/D=0, $0 \le Z/D \le 1.5$) and the lateral cooling effectiveness profiles η along the line (X/D=10, $0 \le Y/D \le 1.5$, Z/D=0) are shown at different levels of the computational grid. Three sets of computation grids with 1.51 million, 2.59 million, and 3.60 million are tested. It is seen that the computational grid with 2.59 million adequately describes the velocity profile near the wall and the local cooling effectiveness distribution over the wall. The predicted results have tiny changes since the computational grid number exceeds 2.59 million. Therefore, the appropriate computational grid number for the cratered hole with arc protrusion is 2.59 million. Similar methods are carried out to obtain the appropriate computational grid numbers for remainder simulations.

The coupled solver is used in ANSYS CFX, which solves the hydrodynamic equations as a single system with a fully implicit discretization. The high-resolution scheme is selected for the advection term. The total energy option is set for the heat transfer model. When the Root Mean Square residuals are less than 10^{-5}, convergence is achieved for the simulation work.

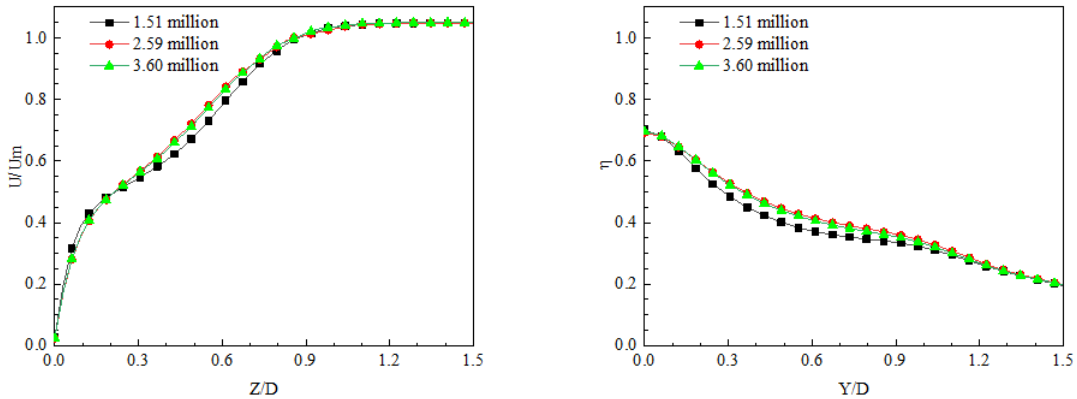

(a) Dimensionless velocity profile **(b) Lateral cooling effectiveness profile**

Fig. 4 Grid independence test for the cratered hole with arc protrusion at M=0.5

2.4 Turbulence model validation with literature data

Two turbulence models, k-ε and SST (Shear Stress Transfer), were chosen for the study to validate the experimental data for the cylindrical hole, elliptical cratered hole (Case 1) and contoured cratered hole in [18] and [29]. Note that all boundary conditions of the numerical simulation are set according to the corresponding experimental conditions. Fig. 5 shows the laterally-averaged cooling effectiveness as a function of the dimensionless downstream distance for both turbulence models at M=0.5. As shown in Fig. 5, the general trend of CFD prediction of the SST turbulence model agrees with the experimental results and gives good quantitative agreements. Therefore, the SST turbulence model was applied to the CFD simulations for the four variants of cratered holes in the current study.

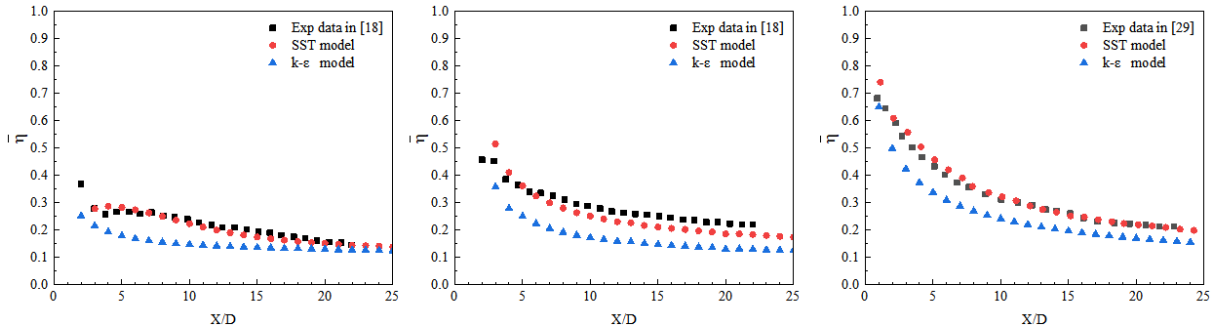

(a) Cylindrical hole **(b) Elliptical cratered hole** **(c) Contoured cratered hole**

Fig. 5 Comparison of numerical simulations with experimental data for different turbulence models

3. Result and Discussion

3.1 Local and area-averaged cooling effectiveness

The contours of cooling effectiveness over the wall surfaces are shown in Fig. 6 for the four cratered holes at blowing ratios M=0.5-2.5. At the lowest blowing ratio, M=0.5, the ejected coolants for either cratered hole are mainly concentrated around the centreline downstream of the crater exit. As the streamwise distance increases, the coolant concentration weakens due to the mixing effect of the hot air. Because the mutual influence between the protrusion and the ejected coolant is relatively weak, there is little effect of the protrusion shape on the local cooling effectiveness distribution at M=0.5. When the blowing ratio has a low or high value, i.e., M=1.0-2.5, the protrusion shape significantly influences the coolant coverage over the wall surface. The coolant coverage at M=1.0 is improved for the cratered holes with arc and triangle protrusions, compared with that at M=0.5, especially over the crater exit region far downstream. However, the cratered hole with trapezoid protrusion at M=1.0 gives an improved coolant concentration around the centreline but worsens lateral coolant coverage. The rectangle protrusion model at M=1.0 provides a remarkable deterioration on the streamwise and lateral coolant coverage over the region X/D>5. As the blowing ratio increases, the worst coolant coverage occurs at M=1.5 for the rectangle protrusion model but M=2.0 for the trapezoid

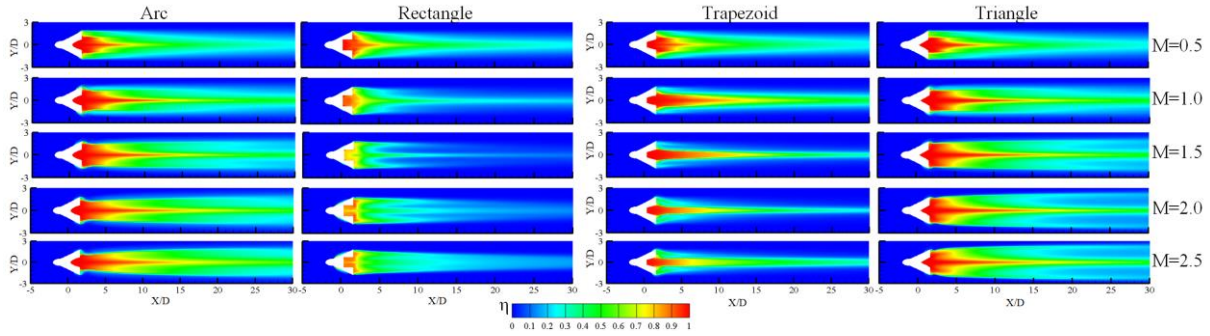

Fig. 6 Local cooling effectiveness distribution at M=0.5-2.5

protrusion model. The arc and triangle protrusion models have minor changes in the coolant coverage but different changes in the detailed distributions of cooling effectiveness. Comparatively, the area with high values of cooling effectiveness for the arc protrusion model gradually increases with the increase of blowing ratio. However, two regions with low values of cooling effectiveness, firstly occurring at M=1.5, gradually enlarges until the blowing ratio achieves 2.5. The arc and triangle protrusion models exhibit better coolant coverages than the cratered holes with rectangle and trapezoidal protrusions.

Fig. 7 shows the centreline cooling effectiveness variations with the streamwise distance at M=0.5-2.5. The profile of centreline cooling effectiveness along the streamwise distance exhibits a monotonic decreasing trend for either cratered hole at either blowing ratio studied. Comparatively, the arc and triangle protrusion models always have the higher cooling effectiveness along the centerline, and the rectangle protrusion model provides the lowest value. The streamwise expansion capability can be explained by comparing the centerline cooling effectiveness values at the same streamwise location. The arc and triangle protrusion models with higher values of cooling effectiveness at X/D=30 indicate better streamwise expansion capabilities. Furthermore, the difference among the centerline cooling effectiveness profiles is small at M=0.5, while a larger difference occurs at other blowing ratios M=1.0-2.5. As the blowing ratio increases, the centerline cooling effectiveness decreases for the cratered hole with rectangle protrusion but increases for the cratered holes with arc and triangle protrusions. The centerline cooling effectiveness for the trapezoid protrusion model increases at the M=0.5-1.0 but decreases at a further larger blowing ratio.

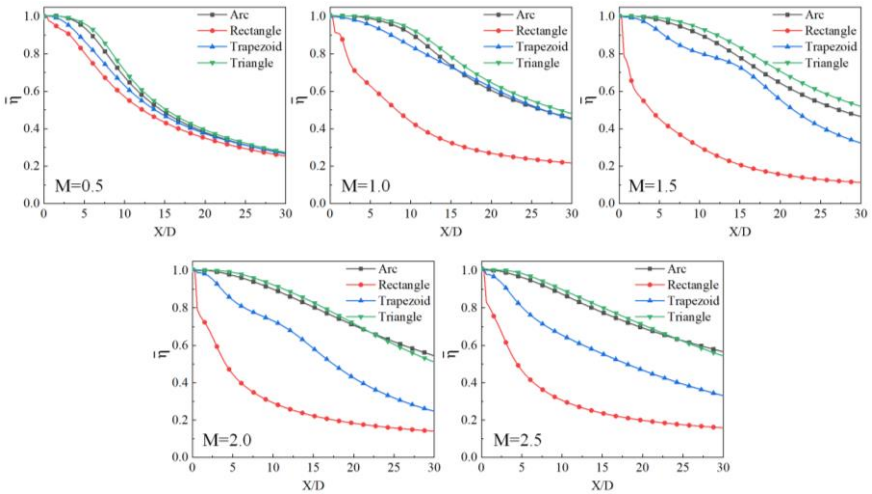

Fig. 7 Centreline cooling effectiveness distributions

Fig. 8 represents the variations of lateral cooling effectiveness at two streamwise locations X/D=5, 10 under the conditions of two blowing ratios M=1.0 and 2.0. At the blowing ratio M=1.0, the lateral cooling effectiveness profiles of all the cratered holes studied show a similar inverted-V shape over one pitch at locations X/D=5 and 10. There is not much difference between the lateral cooling effectiveness profiles for the arc and triangle protrusion models at M=1.0. Comparatively, the rectangle protrusion model provides the smallest lateral cooling effectiveness, and the arc and triangle protrusion models have the higher lateral cooling effectiveness. The trapezoid protrusion model has the worst lateral coolant coverage. The same trends hold at locations X/D=5 and 10 under the blowing ratio M=1.0. When the blowing ratio increases to M=2.0, the arc and triangle protrusion models still give the higher lateral cooling effectiveness and better coolant lateral coverage. Comparatively, the triangle protrusion model has lower cooling effectiveness but wider coolant coverage. The increase of blowing ratio leads to a larger difference in the cooling effectiveness distribution between these two models. For the trapezoid protrusion model, a sharp peak with high cooling effectiveness values occurs near the centerline, and the cooling effectiveness is significantly reduced towards the sideways. For the rectangle protrusion model, the cooling effectiveness distribution profile is fundamentally changed with the increase of blowing ratio, from a single peak at M=1.0 to the three peaks at M=2.0. However, the values of its cooling effectiveness at M=2.0 are more even along the lateral span but reduced, compared with those at M=1.0. Furthermore, the changing trends of the lateral cooling effectiveness distribution at location X/D=10 are almost similar to those at location X/D=5 but generally move down with lower cooling effectiveness.

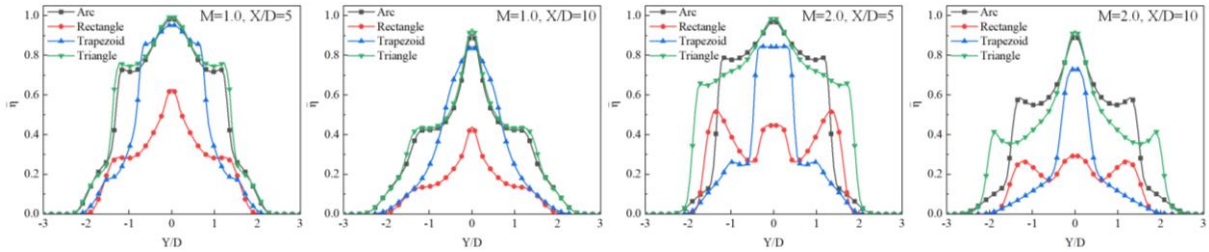

Fig. 8 Lateral distributions of local cooling effectiveness

Fig. 9 represents the variations of the laterally-averaged cooling effectiveness with the streamwise distance for M=0.5-2.5. X/D=0 is inside the crater, which is less affected by the film cooling, resulting in a low cooling effectiveness here. The laterally-averaged cooling effectiveness behind the film hole is decreasing along the streamwise. The laterally averaged film cooling effectiveness of both the arc protrusions and the triangular protrusions essentially increases with the increase of the blowing ratio. The advantage of the triangular protrusion is reflected in the upstream part of the cooling effectiveness region ($2\leq X/D\leq 10$), when the blowing ratio $M\geq 1.0$, the middle and downstream parts ($10\leq X/D\leq 30$) are not greatly influenced by the blowing ratio. While the arc protrusion of the more influenced by the blowing ratio of the region in the middle and downstream part ($10\leq X/D\leq 30$), the laterally-averaged cooling effectiveness with the increase of the blowing ratio continues to rise. Notice that the arc protrusion has a lower cooling effectiveness at the position $2\leq X/D\leq 8$ when the blowing ratio exceeds 2.0. Corresponding to the same position of the arc protrusion hole exit in Fig. 6, the large momentum causes the coolant here to approach the centerline, weakening the coverage effect and making the lateral cooling effectiveness lower. Rectangular protrusions and trapezoidal protrusions in the blowing ratio M>1.0 laterally-averaged lower cooling effectiveness and with the further increase in the blowing ratio cooling effectiveness value changes in a small range.

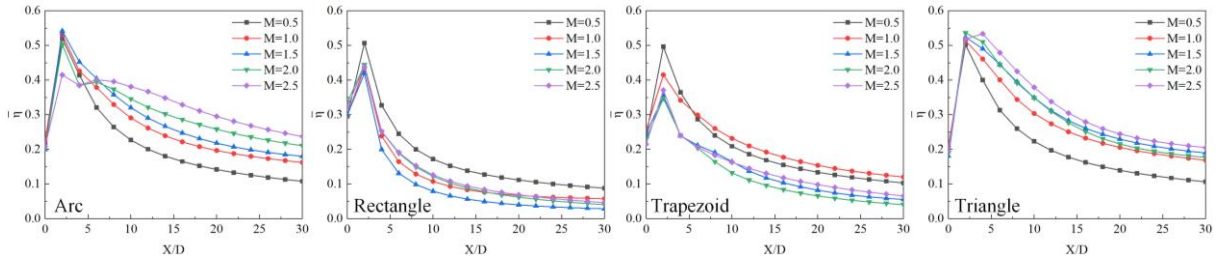

Fig. 9 Laterally-averaged film cooling effectiveness

Fig. 10 represents the area-averaged cooling effectiveness for the four protrusion models at M=0.5-2.5. The predicted performance of the traditional cylindrical film cooling hole with an inclination angle of 30º is also provided as the benchmark. It is concluded that all shaped protrusion models have higher area-averaged cooling effectiveness than the baseline cylindrical hole at the blowing ratios studied. Both the arc and triangle protrusion models have continuous increase trends of area-averaged cooling effectiveness in general with the increase of blowing ratio. The only exception occurs for the triangle protrusion model at M=2.0 with a slight decrease in the area-averaged cooling effectiveness. As seen from the local cooling effectiveness distribution in Fig. 6, the bilateral regions with lower cooling effectiveness at $15 \le X/D \le 30$ exhibits a higher area at M=2.0 than those at M=1.5, resulting in a reduction of are-averaged cooling effectiveness. However, the reduction at the far downstream region is overcome by the enhancement in the region just downstream the hole exit $0 \le X/D \le 10$. Furthermore, the triangle protrusion model has slightly higher area-averaged cooling effectiveness than the arc protrusion model at M=1.0 and 1.5 but slightly lower values at the other three blowing ratios. The rectangle and trapezoidal protrusion models yield lower area-averaged cooling effectiveness than the arc and triangle protrusion models, and the margins are greater with the increase of blowing ratio. The rectangular protrusion model has the worst area-averaged cooling effectiveness among the four protrusion models. However, it still provides a 50.13% improvement compared to the benchmark cylindrical hole at M=0.5, and this improvement becomes more pronounced as the blowing ratio increases.

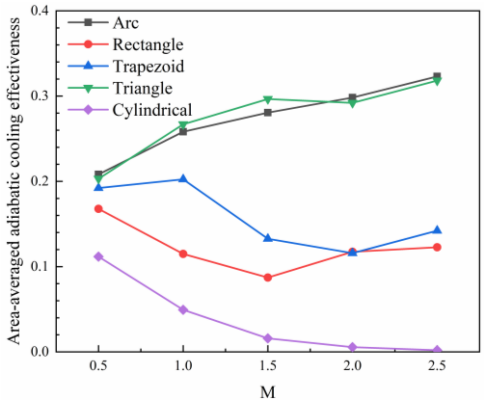

Fig. 10 Area-averaged cooling effectiveness at various blowing ratios

3.2 Flow field

To better explain the reason for the difference in local cooling effectiveness distribution between the four protrusion cratered holes, the contours of streamwise vorticity, and the surface streamlines on planes X/D=5 at blowing ratios M=1.0 and 2.0 are shown in Fig. 11, also the corresponding 3D vortex

structures are given in Fig. 12. And the coolant flow in the *Z-X* section view at *Y/D*=0.0 position for the four protruding cratered holes at blowing ratios *M*=1.0, 2.0 are shown in Fig. 13.

At the blowing ratio *M*=1.0, the arc and triangle protrusion cratered holes represent similar streamwise vorticity structures and intensities, including three vortex pairs. The flow field with three vortex pairs is different from that with two vortex pairs in [24-26], mainly attributed to a larger lateral span of 6*D* in the current study. The middle one is the original kidney-shaped vortex pair, commonly regarded as the origin of the coolant lift-off. For the arc and triangle protrusion models, the original kidney-shaped vortex pair is suppressed just near the centerline by the anti-kidney-shaped vortex pair sideways in the regions ($-1.5 \le X/D \le -0.5$, $0.5 \le X/D \le 1.5$), hence better coolant coverages can be achieved in the relevant regions. The anti-kidney vortex pair is induced by the interaction between the protrusion and ejected coolant, as explained by Bai and Zhang [24]. The third vortex pair has an opposite rotation direction to the anti-kidney-shaped vortex, generated by the ejected coolant between the mainstream at the sideways. This side kidney-shaped vortex pair is detrimental to the coolant spreading laterally. As shown in Fig. 13, this vortex structure at lower blowing ratios causes most of the coolant to adhere to the walls, which has a positive effect on the cooling of the walls. For the rectangle protrusion model, it is seen that the large-scale kidney-shaped vortex pair dominates the whole lateral region, resulting in the worst coolant coverage. This means that the rectangle protrusion has little impact on the kidney-shaped vortex pair than the benchmark cylindrical hole. For the trapezoidal protrusion model, the side kidney-shaped vortex vanishes, and the anti-kidney-shaped vortex pair is underneath the middle kidney-shaped vortex pair. Therefore, the improvement of lateral coolant coverage is limited but a significant enhancement in the region around the centerline. Fig. 13 demonstrates the tendency of most of the coolant in the middle and downstream of the rectangular protrusion to move away from the wall, causing the coolant downstream to move away from the wall and reducing the effectiveness of film cooling. Although the trapezoidal protrusion has improved coolant coverage over the rectangular protrusion, there is still a larger portion of coolant downstream that is off the wall.

When the blowing ratio increases to 2.0, the kidney-shaped and anti-kidney-shaped vortex pairs have enlarged scales and increased intensities for all cratered holes. The flow structure for the rectangle protrusion model is still the dominated kidney-shaped vortex pair, resulting in the worst coolant coverage in accordance. For the trapezoidal model, the underneath anti-kidney-shaped vortex pair is squeezed remarkably near the centerline by the preponderant kidney-shaped vortex pair, which induces a poor lateral coolant coverage. This means that insufficient anti-kidney-shaped vortex pair cannot overcome the negative effect of the kidney-shaped vortex pair. For the flow of coolant in Fig. 13, the increased blowing ratio causes the flow velocity of coolant in the hole to rise significantly. The rectangular and trapezoidal protrusion structure allows a large amount of coolant to be lifted further away from the wall surface, thus having a significant negative impact on the coolant coverage of the downstream wall surface and greatly reduces the cooling effectiveness on the wall surface. Comparatively, the size and intensity of the anti-kidney-shaped vortex pairs are still overwhelming in the flow field for both arc or triangular protrusion models, and the coolant flow shown in Fig. 13 indicates that the coolant still maintains better coverage on the walls of both protrusion models. The good lateral coolant coverage in Fig. 6 also shows this. The anti-kidney-shaped vortex pair for the triangle protrusion model occupies a wider lateral region than that for the arc protrusion model, resulting in a wider profile with higher cooling effectiveness, shown in Fig. 8.

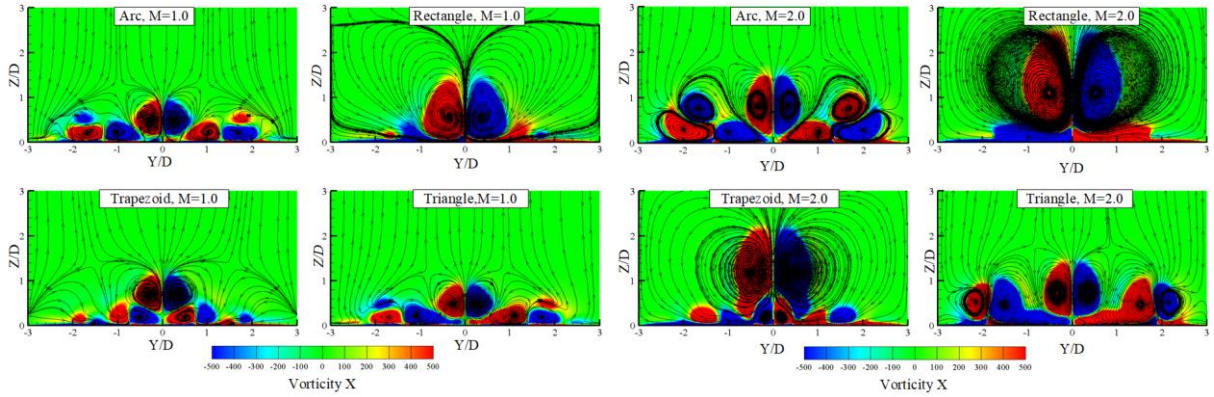

Fig. 11 Contour of streamwise vorticity and surface streamlines over plane *X/D*=5

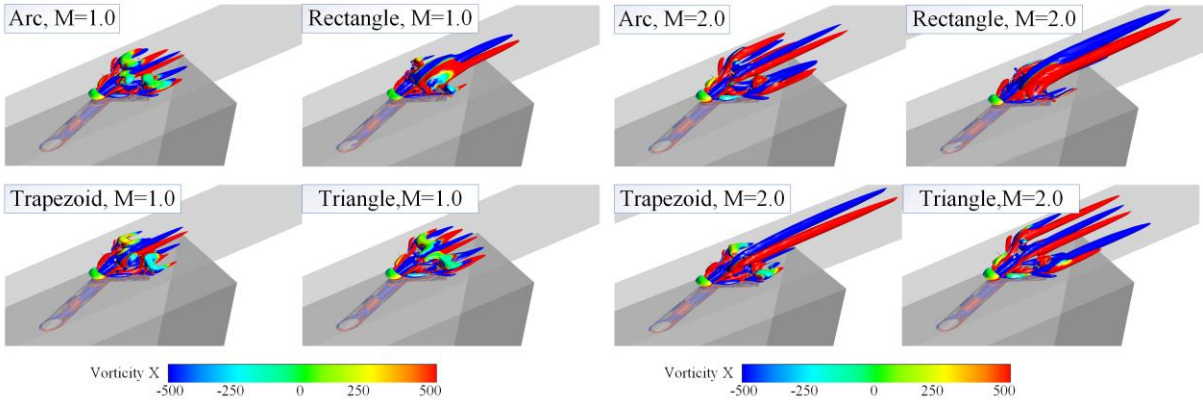

Fig. 12 3D vortex structures (Numerical simulated isosurfaces of Velocity. Invariant Q=10^6)

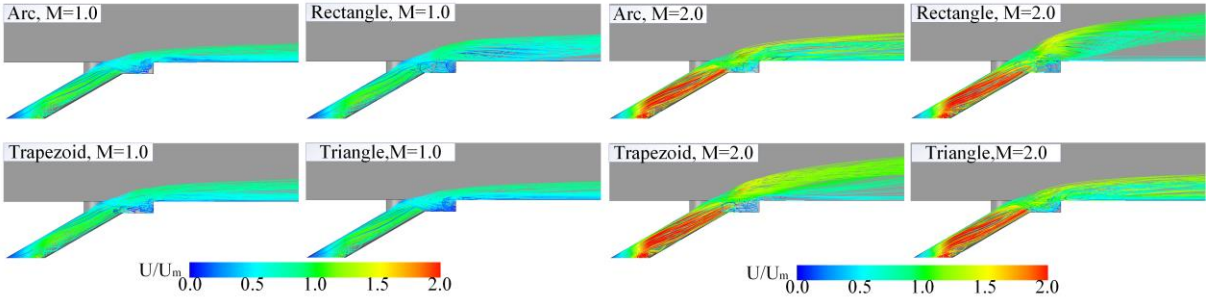

Fig. 13 Flow field in the *Z-X* section view at *Y/D*=0.0

3.3 Total pressure loss coefficient

The aerodynamic loss performances for the cratered holes studied are represented in Fig. 14. The total pressure loss coefficients for each protrusion model increase monotonously with the blowing ratio from 0.5 to 2.5. Compared with the benchmark cylindrical hole, the cratered holes exhibit higher aerodynamic loss, mainly attributed to the interaction between the crater and coolant in the hole, as explained by Zhang et al. [27]. However, the specific total pressure loss coefficient depends on the protrusion shape. In comparison, the rectangular protrusion model gives the largest total pressure loss coefficient, increasing by 13.81% at *M*=2.5 compared to the benchmark cylindrical hole, and the other three protrusion models increased by 6.13%-7.56%. Combined with the area-averaged cooling effectiveness in Fig. 10, the rectangle protrusion model has the worst overall performance due to its

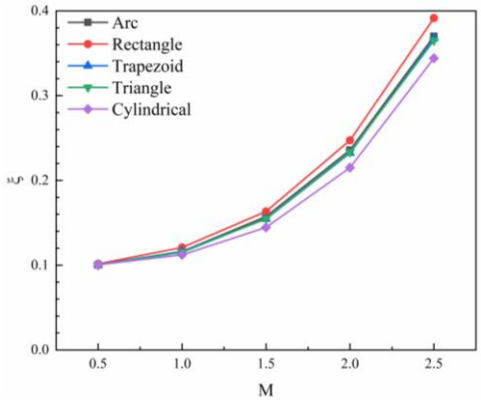

Fig. 14 Total pressure loss coefficients

lowest area-averaged cooling effectiveness and highest aerodynamic loss. The arc and triangle protrusion models are recommended, as they provide higher area-averaged cooling effectiveness and lower total pressure loss coefficients.

4. Conclusion

The present study numerically studied the cooling effectiveness, flow structure, and total pressure loss coefficients for the flat-plate film cooling with contoured cratered holes. Four protrusion shapes, including arc, rectangle, trapezoidal, and triangle, for the cratered holes, are considered. The simple cylindrical hole is also investigated as the benchmark. Based on the result discussion, the main conclusions are drawn as follows:

1) The protrusion shape has a limited effect on the local and area-averaged cooling effectiveness for the contoured cratered film-cooling holes at a blowing ratio of M=0.5 but leads to a quite different cooling performance at blowing ratios M=1.0-2.5. The arc and triangle protrusion models improve the cooling performance, especially at higher blowing ratios.
2) The rectangle protrusion model generates no anti-kidney-shaped vortex pair, resulting in the worst coolant lateral coverage. The arc and triangle protrusion models produce the additional anti-kidney-shaped vortex pair with sufficient scale and intensity, leading to considerable improvements of the lateral coolant coverage.
3) Various protrusion shape contributes to a different aerodynamic loss coefficient for the cratered film-cooling hole. Comparatively, the rectangle protrusion model has a significantly higher total pressure loss coefficient than the other three protrusion models.

Acknowledgment

This work was supported by the National Natural Science Foundation of China (Grant No. 51976139).

Nomenclature

D – Film-cooling hole diameter, [mm]
M – Blowing ratio, [$=DR(U_c/U_m)$], [–]
m_c – Mass flow rate of the coolant, [kgs^{-1}]
m_m – Mass flow rate of the mainstream hot gas, [kgs^{-1}]
$P_{t,cin}$ – Total pressure at the inlet of cooling hole, [Pa]
$P_{t,m}$ – Total pressure at the inlet of mainstream channel, [Pa]
$P_{t,f}$ – Total pressure at the outlet of mainstream channel, [Pa]
T – Temperature, [K]
T_{aw} – Adiabatic wall temperature, [K]
T_c – Coolant temperature, [K]
T_m – Mainstream temperature, [K]
U_c – Velocity at the cross-section of the cylindrical hole, [ms^{-1}]
U_m – Velocity at the inlet of hot gas, [ms^{-1}]
U_Y – Velocity components in the Y directions, [ms^{-1}]
U_Z – Velocity components in the Z directions, [ms^{-1}]
X, Y, Z – Cartesian coordinates, [–]

Greek symbols
η – Adiabatic film cooling effectiveness, [$=(T_m-T_{aw})/(T_m-T_c)$], [–]
ξ – Total pressure loss coefficient, [–]
ρ_m – Density of mainstream channel inlet, [kgm^{-3}]

Abbreviations
DR – Density ratio, [–]
SST – Shear Stress Transfer, [–]

References

[1] Goldstein, R.J., Film Cooling, *Adv. Heat Transf,* (1971), 7, pp. 321-379
[2] Sinha, A.K., *et al.*, Film-cooling effectiveness downstream of a single row of holes with variable density ratio, *ASME J, Turbomach, 113* (1991), 3, pp. 442-449
[3] Goldstein, R.J., *et al.*, Film cooling effectiveness and mass/heat transfer coefficient downstream of one row of discrete holes, *ASME J. Turbomach, 121* (1999), 2, pp. 225-232
[4] Baldauf, S., *et al.*, High-resolution measurements of local effectiveness from discrete hole film cooling, *ASME J. Turbomach, 123* (2001), 4, pp. 758-765
[5] Abdelmohimen, M.A.H, *et al.*, Numerical analysis of film cooling due to simple/compound angle hole combination, *Arabian J. Sci. Eng,* (2020), 45, pp. 8931-8944
[6] Wang, J., *et al.*, Effect of spherical blockage configurations on film cooling, *Therm. Sci., 22* (2018), 5, pp. 1933-1942

[7] Taheria, Y., *et al*., Multi-objective optimization of three rows of film cooling holes by genetic algorithm, *Therm. Sci*., *25*(2021), 5, pp. 3531-3541
[8] Goldstein, R.J., *et al*., Effects of hole geometry and density on three-dimensional film cooling, *Int. J. Heat Mass Transf, 17* (2015), 5, pp. 595-607
[9] Bunker, R.S., A review of shaped hole turbine film-cooling technology, *ASME J. Heat Transf, 127* (2005), 4, pp. 441-453
[10] Ping, D., Feng, L., Numerical study on film cooling effectiveness from shaped and crescent holes, *Numer. Heat Transf, 47* (2011), 2, pp. 147-154
[11] Lee, K.D., Kim, K.Y., Performance evaluation of a novel film-cooling hole, *ASME J. Heat Transf, 134* (2012), 10, Article number. 101702
[12] Kusterer, K., *et al*., Highest-efficient film cooling by improved nekomimi film cooling holes – part 1: ambient air flow conditions, *Proceedings*, ASME Turbo Expo 2013: Turbine Technical Conference and Exposition, San Antonio, Texas, USA, 2013, Vol. 3B, V03BT13A040
[13] Tian, K., *et al.*, Effect of combined hole configuration on film cooling with and without mist injection, *Therm. Sci*., *22* (2018), 5, pp. 1923-1931
[14] Krishna A.V.G., Parammasivam K.M., Thermal barrier coated surface modifications for gas turbine film cooling: a review, *J. Therm. Anal. Calorim, 146* (2021), 5, pp. 545–580
[15] Bunker, R.S., Film cooling effectiveness due to discrete holes within a transverse surface slot, *Proceedings*, ASME Turbo Expo 2002: Power for Land, Sea, and Air, Amsterdam, Netherlands, (2002), Vol. 3, pp. 129-138
[16] Fric, T.F., Campbell, R.P., Method for improving the cooling effectiveness of a gaseous coolant stream which flows through a substrate, and related articles of manufacture, *U.S. Patent*, (2002), No. 6383602
[17] Tran, N., *et al*., Prediction of adiabatic effectiveness of various cratered film hole configurations: sensitivity analysis for the rectangle shaped mask, https://arc.aiaa.org/doi/pdf/10.2514/6.2010-404
[18] Lu, Y., *et al*., Film cooling measurements for cratered cylindrical inclined holes, *ASME J. Turbomach, 13*1 (2009), 1, pp. 43-54
[19] Khalatov, A., *et al*., Application of cylindrical, triangular and hemispherical dimples in the film cooling technology, *J. Phys.: Conf. Ser, 891* (2017), 1, Article number. 012145
[20] Khalatov, A., *et al*., Film cooling evaluation of a single array of triangular craters, *Int. J. Heat Mass Transf, 159* (2020), Article number. 120055
[21] Kalghatgi, P., Acharya, S., Improved film cooling effectiveness with a round film cooling hole embedded in contoured crater, *ASME J. Turbomach, 137* (2015), 10, Article number. 101006
[22] Kalghatgi, P., Acharya, S., Flow dynamics of a film cooling jet issued from a round hole embedded in contoured crater, *ASME J. Turbomach, 141* (2019), 8, Article number. 081006
[23] An, B.T., Film cooling effectiveness measurements of a near surface streamwise diffusion hole, *Int. J. Heat Mass Transfer, 103* (2016), pp. 1-13
[24] Bai, L.C., Zhang, C., Flow mechanism of cooling effectiveness improvement for the cylindrical film cooling hole with contoured craters, *IOP Conf. Ser.: Mater. Sci. Eng. 473* (2019), 1, Article number. 012033
[25] Fu, J.L., *et al*., Film cooling performance for cylindrical holes embedded in contoured craters: effect of the crater depth, *J. Appl. Mech. Tech. Phys, 60* (2019), 6, pp. 1068-1076

[26] Bai, L.C., *et al*., Optimization of geometric parameters of cylindrical film cooling hole with contoured craters to enhance film-cooling effectiveness, *Thermophys. Aeromech, 28* (2021), 6, pp. 835-848
[27] Zhang, C., *et al*., Discharge coefficients and aerodynamic losses for cylindrical and cratered film-cooling holes with various coolant crossflow orientations, *J. Braz. Soc. Mech. Sci. Eng, 43* (2021), 3, Article number, 161
[28] Menter, F.R., Two-equation eddy-viscosity turbulence models for engineering applications, *AIAA J, 32* (1994), 8, pp. 1598-1605
[29] Bai, L.C., Research on optimization design and thermal coupling analysis of the cratered hole, Master thesis, Tianjin University of Technology, Tianjin, CHINA, 2021
[30] Aga, V., *et al*., Aerothermal performance of streamwise and compound angled pulsating film cooling jets, *J. Turbomach*, *131*(2009), 4, Article number, 041015

Received: 15.04.2022.
Revised: 02.07.2022.
Accepted: 01.08.2022.